

Gravitational Quenching by Clumpy Accretion in Galaxies and Clusters II: Dynamical Response to Heating

Yuval Birnboim^{1,2}, Avishai Dekel²,

¹*Harvard Smithsonian Center for Astrophysics, 60 Garden Street, Cambridge, MA 02138 USA*

²*Racah Institute of Physics, The Hebrew University, Jerusalem 91904 Israel*

ybirnboim@cfa.harvard.edu; dekel@phys.huji.ac.il

3 May 2022

ABSTRACT

Galaxy clusters pose a “cooling-flow problem”, where the X-ray emission from their cores is not accompanied by enough cold gas or star formation. This requires a continuous energy source that balances the cooling rate over the whole core volume. We address the feasibility of a gravitational heating mechanism, utilizing the gravitational energy released by the gas that streams into the potential well of the cluster dark-matter halo. We focus here on a specific form of gravitational heating in which the energy is transferred to the medium thorough the drag exerted on inflowing gas clumps. Using spheri-symmetric hydro simulations with a subgrid representation of these clumps, we confirm our earlier estimates that in haloes $\geq 10^{13} M_{\odot}$ the gravitational heating is more efficient than the cooling everywhere. The worry was that this could overheat the core and create an instability that might push it away from equilibrium. However, we find that the overheating does not change the global halo properties, and that convection can stabilize the cluster by carrying energy away from the overheated core. In a typical rich cluster of $10^{14-15} M_{\odot}$, with $\sim 5\%$ of the accreted baryons in gas clumps of $\sim 10^8 M_{\odot}$, the simulated temperature and entropy profiles are consistent with those observed in cool-core clusters, and so are the predicted density and mass of cold gas and the level of turbulence.

Key words: galaxies: clusters: general — galaxies: haloes — (galaxies:) cooling flows — galaxies: formation — hydrodynamics — X-rays: galaxies: clusters

1 INTRODUCTION

Galaxy clusters can be divided into two distinct populations according to the X-ray luminosity of their central cores (Sanderson et al. 2006). Cool-core (CC) clusters are centrally concentrated, highly luminous in X-ray, and have central cooling times of 0.1 – 1 Gyr. Non-cool-core (NCC) clusters have lower densities and luminosities near the centre, and their central cooling times are typically a few Gyrs (Donahue et al. 2006). The population of CCs has little internal variability, and they all exhibit a typical temperature profile with a decline by a factor of 2-3 in the innermost few 10 kpc (Leccardi & Molendi 2008). Based on the short cooling time in CCs, one expects to observe gas in intermittent temperatures, a high star-formation rate in the brightest central galaxy (BCG) ($\gtrsim 100 M_{\odot}/\text{yr}$), and a large stellar mass in the BCG ($10^{12-13} M_{\odot}$), none of which is observed. These are three manifestations of the cooling-flow problem in clusters (Fabian 1994). Since the cooling time is inferred directly from observations based on the

luminosity and temperature, the discrepancy between the expected cooling rates and the gas that actually cools indicates that some heating mechanism is keeping the gas hot in a stable configuration.

Several mechanisms have been proposed as potential solutions to the cooling-flow problem. Most popular is AGN feedback, where energy or momentum are provided by an active galactic nucleus either in an intense quasar mode (Ciotti & Ostriker 2007), in a slower radio mode (Best 2007; Cattaneo et al. 2009, and reference within), or via cosmic rays (Guo & Oh 2008). The AGNs clearly release sufficient power to balance the cooling in the core, but the coupling to the gas in the whole core volume is not easily understood, and the requirement of continuous heating is not a trivial constraint (De Young et al. 2008).

Alternatively, one can utilize the fact that the gravitational power released as fresh baryons stream into the potential well created by a massive halo is more than enough to balance the cooling rate at the centre

(Fabian 2003; Dekel & Birnboim 2008; Wang & Abel 2008). Among the mechanisms through which this energy is transferred to the inner halo one could consider thermal conduction Kim & Narayan (2003), turbulence (Sato & Nagataki 2004), and dynamical friction (El-Zant et al. 2004; Faltenbacher & Mathews 2007; Naab et al. 2007; Khochfar & Ostriker 2008; Johansson et al. 2009). In particular, the turbulence induced by accreting sub-structures may disturb the magnetic field in a way that could make the conduction more efficient (Ruszkowski & Oh 2010).

The gravitational power that is released during the streaming of baryons into clusters of $M \geq 10^{13} M_{\odot}$ is indeed sufficient for balancing the expected radiative losses (Dekel & Birnboim 2008, hereafter DB08). The challenge is to deposit this energy at the inner cluster core of $\sim 30 - 100$ kpc, where most of the cooling takes place. The energy should be evenly distributed over the whole core volume and continuously over several Giga years. It should be performed in a way that is consistent with the observed entropy (Donahue et al. 2006) and metallicity (Rebusco et al. 2006) profiles. Here we investigate a model in which some of the accreted gas is in dense and cold ($\sim 10^4$ K) gas clumps. These clumps do not stop at the virial shock but rather penetrate to the inner parts of the halo. The continuous accretion of many clumps through the halo can distribute the energy smoothly in a large volume, as required, as opposed to AGN feedback that is episodic and originates from a very small region near the black hole. The main physical mechanism that couples the clumps and the halo gas is hydrodynamic drag, subsonic or supersonic, which decelerates the clumps and causes the deposition of their kinetic and potential energy in the ambient medium. Hydrodynamic drag is more efficient when the clumps are smaller and moving faster, as opposed to dynamical friction that becomes more efficient for more massive clumps and for transonic velocities (Ostriker 1999). We pointed out in DB08 that the gravitational heating is likely to be associated with the streams that build the cluster along the filaments of the cosmic web. These streams could transfer their energy to the cluster core via the generation of turbulence and other mechanisms that are not necessarily associated with cold clumps (Zinger et al. 2010). Still, the heating through cold clumps is a concrete example that allows a simple study of the dynamical response with general implications that are not limited to this particular coupling mechanism.

In DB08 we showed that accreted clumps could balance the cooling in haloes more massive than $6 \times 10^{12} M_{\odot}$, provided that the clumps contain a non-negligible fraction of the infalling gas ($\geq 10\%$ for a $10^{15} M_{\odot}$ halo), and that the clump masses are in the range $10^4 - 10^8 M_{\odot}$. The clumps heat the intra-cluster medium (ICM) via drag until they disintegrate by hydrodynamical instabilities (Murray & Lin 2004; Maller & Bullock 2004). The permitted mass range for the clumps took into account additional criteria for clump survivability, such as Bonnor-Ebert instability, conduction and evaporation. When these conditions are met, the clumps survive long enough to penetrate

through the outer halo and reach the centre, but their interaction with the ICM is sufficiently strong for most of the clump energy to be deposited in the core within a Hubble time. In this paper we implement the basic features that were investigated statically in DB08 in a dynamical evolving configuration.

The heating rate by drag (and by other mechanisms such as dynamical friction, cosmic rays from AGN) is proportional to the density of the hot ambient gas, $\dot{e}_{\text{heat}} \propto \rho_{\text{hot}}$. On the other hand, the Bremsstrahlung cooling rate per unit volume scales like $\dot{e}_{\text{cool}} \propto \rho_{\text{hot}}^{1.5}$ (assuming isobaric gas). This generates an instability through a positive feedback loop (Field 1965; Conroy & Ostriker 2008). A small negative density perturbation, e.g., produced by gas expansion due to overheating, would make the ratio of heating to cooling rate increase as $\dot{e}_{\text{cool}}/\dot{e}_{\text{heat}} \propto \rho_{\text{hot}}^{0.5}$, leading to more overheating, enhanced pressure, and a runaway expansion. An analysis of the consequences of this instability, and an investigation of possible mechanisms that could keep the cluster in equilibrium, necessitate a dynamical treatment.

This unstable overheating, as reproduced in spherically-symmetric simulations below, results in expanding shells that heat to temperatures as high as 10^9 K, clearly at odds with observations. In the real world, this overheating must be regulated by processes that smooth temperature or entropy gradients by heat transfer through conduction or convection. Conduction is suppressed in the presence of magnetic fields (Fabian 1994, and reference within), though it might be boosted almost to its maximum possible value (Spitzer 1962) by turbulence (Narayan & Medvedev 2001; Balbus & Reynolds 2008; Ruszkowski & Oh 2010), which might be a natural product of clump heating. Convection is a promising mechanism for smoothing the local instabilities. In the simple case of an ideal gas with a uniform chemical composition in a spherical potential well, convection occurs in regions where the entropy is declining with radius. However, the strength of this convection is uncertain, as it depends on the gradients in gas properties and on the magnetic fields. Weak magnetic fields make the gas more susceptible to convection, with the entropy-gradient criterion replaced by the temperature gradient (Parrish et al. 2008), but for certain types of perturbations, the convection strength might be drastically suppressed by effects related to magnetic tension (Parrish et al. 2008, 2009). Regardless of the actual energy transport mechanism, one expects nature not to permit shells of $\sim 10^9$ K in close contact with shells of $\sim 10^7$ K, and to act to smooth such a discontinuity. Motivated by the turbulence that is expected to be generated by the clumps, we focus below on convection as the mechanism that smooths steep gradients, but we expect the final profiles to be qualitatively similar when the mechanism for energy transport is conduction because smooth entropy and pressure (the result of convection) is equivalent to smooth temperature and pressure (the result of conduction).

In this paper, we mimic this smoothing process by a 1D mixing-length convection model (Spiegel 1963), with

a the mixing-length coefficient L the single free parameter. We find that the results are almost independent of the value of this parameter as long as noticeable convection occurs. This allows us to further simplify the model by assuming that the convection is maximal, namely the energy transfer rate is limited by the requirement that hot bubbles accelerate until they become supersonic, at which point they disintegrate. This leaves us with no free parameters in our convection model.

There are some additional benefits from a dynamic treatment of the clump heating process. The analysis of DB08 considered simple Monte-Carlo clump trajectories within an otherwise static halo in hydrostatic equilibrium. This assumption of a static halo could be valid for one Gigayear but the cluster may evolve considerably over a Hubble time, due, for example, to the gradual increase of virial temperature and the growth of the BCG. Furthermore, if clump heating is taking place, cold clumps continually get destroyed near the halo centre, dumping cold gas near the BCG. This dilution of the hot gas with cold gas is not a problem for the heating-cooling balance because the clumps bring in several times the energy needed for heating themselves to the cluster virial temperature, but a proper account of this clump deposition requires a dynamical analysis of an evolving cluster.

In §2 we describe the implementation of the clump model and of the convection model in the 1D hydrodynamic code. In §3 we show results of hydrodynamic cluster simulations with convection and clump heating that match the observed temperature and entropy profiles of clusters and the cooling rates in clusters without a need for any additional feedback. In §4 we address possible direct and indirect observations of the cold clumps. In §5 we summarize and conclude.

2 METHODS

2.1 Implementing Clumps in 1D Hydrodynamic Simulations

According to our estimates in DB08, heating by clumps requires clump masses in the range $10^4 - 10^8 M_\odot$. In order to properly resolve drag forces and clump disintegration via hydrodynamical instabilities, these clumps should be resolved by at least 1000 cells or SPH particles (i.e., 10 cells across each dimension). The implied required dynamical range in a cluster of $10^{14} - 10^{15} M_\odot$ is impractical, so simulation of such clumps requires a sub-grid model. We develop such a model below, and describe its implementation in a 1D spherical hydrodynamical code.

The clumps are made of cold and partly ionized gas at $\sim 10^4$ K in pressure equilibrium with their surrounding hot halo. For a rich cluster of galaxies, with a virial temperature $\sim 10^7$ K, the overdensity within the clumps is about 10^3 . The clumps couple to the hot gas by a drag force

$$f_{\text{drag}} = \frac{1}{2} C_d A \rho_{\text{hot}} v_{\text{rel}}^2, \quad (1)$$

acting opposite to the relative direction of motion. Here

C_d is the drag coefficient (~ 1 for a spherical gas clump), A is the surface area of the clump (πR_{cl}^2), ρ_{hot} is the density of the hot component, and v_{rel} is the relative velocity between the clump and the halo gas. Eq. (1) holds for subsonic and supersonic motions, though the value of C_d may vary, especially in the trans-sonic regime where it could be a few. The deceleration ($f_{\text{drag}}/m_{\text{cl}}$) is proportional to the ratio of clump surface area to volume, $\propto m_{\text{cl}}^{-1/3}$. This dictates lower and upper limits to the relevant clump masses. Clumps that are too small cannot penetrate through the outer halo into the core, and clumps that are to large cannot deposit a significant fraction of their energy in the inner halo on a time scale shorter than the Hubble time.

Single clump simulations (Murray & Lin 2004) indicate that most of the energy dissipated in this process goes into the hot ambient gas. The survivability of these clumps is an open question as they could be destroyed by many different effects. This has been discussed in DB08 and in Maller & Bullock (2004). In a nutshell, if the clump is more massive than $\sim 10^8 M_\odot$ it would exceed the Bonnor-Ebert critical mass (the equivalent of the Jeans mass for pressure-confined spheres) and it would collapse under its self-gravity and turn into stars. If the clump is less massive than $\sim 10^4 M_\odot$, evaporation and conduction are expected to disintegrate the clump. Hydrodynamic instabilities, particularly Kelvin-Helmholtz instability, tend to break the clump, typically after it has repelled the equivalent of its own mass in ambient gas (Murray & Lin 2004). The clump masses then cascade down toward the lower limit for clump mass.

2.1.1 The Hydra Code

Subgrid recipes of the effects mentioned above were incorporated into the 1D spherical code Hydra (Birnboim & Dekel 2003). The code is finite-difference Lagrangian with von-Neumann first and second order artificial viscosity. Dark matter is described as zero-width shells that propagate through the gaseous shells, and interact with them gravitationally. The coupled density fields of gas and dark matter shells are propagated using a 4th order Runge-Kutta method. Time steps are defined by the minimum of the Courant conditions and the allowed deviation of the forth order scheme from fully explicit (1st order) time step. When this difference exceeds some preset epsilon, the previous values are restored, and a new step with decreased time step is performed.

The baryons and the dark matter shells are assigned a preset angular momentum that is added as an impulse when the shell is at its turn-around. This prevents a numerical and physical singularity at the centre. The angular momentum of the dark matter is set so that the rotational kinetic energy is 18% of the radial kinetic energy at the virial radius. The results are insensitive to this choice. The baryonic angular momentum is set to produce a spherical, angular-momentum supported “disc” of radius ~ 10 kpc for a cluster halo of $10^{15} M_\odot$, to mimic a BCG. Since centrifugal forces

scale like r^{-3} , the angular momentum of the baryons is negligible at a distance comparable to a few disc radii above the disc. We note that a spherical code is not the right tool for studying disc formation, and this setup is essentially an inner boundary condition for the halo simulation. In addition, the code imposes a central smoothing length on the gravitational acceleration, $a_g = G M / (r + s)^2$, typically with $s \sim 50$ pc. Radiative cooling is calculated by a metallicity dependent cooling function (Sutherland & Dopita 1993) with a constant preset metallicity.

The initial conditions, in terms of shell masses, radii and peculiar velocities, were set at $z = 100$ such that the future accretion rate onto the growing halo will follow a desired accretion rate (Dekel 1981; Birnboim & Dekel 2003, appendix C). Specifically, the initial perturbation used here yields an accretion history that traces that of an average main progenitor according to the EPS approximation Press & Schechter (1974); Lacey & Cole (1993); Neistein et al. (2006). The procedure is described in detail in Birnboim et al. (2007). The code has been compared successfully to analytic predictions of Bertschinger (1985) and to a Von-Neumann-Sedov-Taylor problem. The Courant conditions and epsilon are set so that the global energy conservation over a Hubble time is always better than 1% and the spatial convergence was tested for each set of simulations. Timesteps are consequently $\sim 10^{-5}$ Gyr throughout most of the simulation.

2.1.2 Drag forces in 1D

The subgrid model for clumps is similar in its approach to “sticky particle” techniques in the sense that it calculates subgrid interactions on otherwise N-body particles. Here we define “clump-shells”, which, like dark matter shells, are able to penetrate through baryonic shells. The clump shells are assigned some angular momentum (similarly to the baryon and dark matter shells) that stops them from reaching the singularity at the centre. Clump shells typically oscillate around the halo’s centre before the processes described below destroy them.

Each shell is assumed to contain n_{cl} clumps with mass

$$m_c = \frac{M_{\text{shell}}}{n_{\text{cl}}}. \quad (2)$$

M_{shell} and m_c are the total shell mass and the mass of each gaseous clump respectively. The shells interact with the baryons by decelerating according to eq. (1). The drag force equation and energy equation of an interaction between some clump i and a parcel of gas are:

$$f_{\text{cl}}^i = -F_{\text{gas}}^i, \quad (3)$$

and

$$\dot{E}^i = f_{\text{cl}}^i v_{\text{cl}}^i + F_{\text{gas}}^i u_{\text{gas}} + Q^i = 0, \quad (4)$$

respectively with f_{cl}^i and F_{gas}^i the forces on the clump and gas parcels arising from the clump-gas interactions, and v_{cl}^i and u_{gas} the velocities of clump i and the gas

respectively. We assume that many clumps are present within each parcel of gas, and that their motions are isotropic so their forces cancel out:

$$\sum F_{\text{gas}}^i = 0, \quad (5)$$

and

$$\begin{aligned} \dot{E}_{\text{tot}} &= \sum f_{\text{cl}}^i v_{\text{cl}}^i + \sum F_{\text{gas}}^i u_{\text{gas}} + \sum Q^i \\ &= \sum f_{\text{cl}}^i v_{\text{cl}}^i + \sum Q^i = 0. \end{aligned} \quad (6)$$

In the reference frame of a gas parcel, the clump loses energy, which is converted to heat, so using eq. (1) we identify

$$Q^i = f_{\text{drag}} v_{\text{rel}} = \frac{1}{2} C_d A \rho_{\text{hot}} |v_{\text{rel}}|^3, \quad (7)$$

as the heating rate that clump i heats the gas parcel in which it is embedded. The total energy of the clumps and of the gas should be conserved on average according to eq. (6). Assuming there are enough clumps so the averaging is correct, and that the assumption that the clumps have isotropic velocities is good. The difference equations in Hydra conserve energy algebraically¹ (making energy conservation independent of resolution), and we do not want to violate this property. We thus require a detailed balance between the clump deceleration and energy deposition of each clump:

$$f_{\text{cl}}^i v_{\text{cl}}^i = Q^i, \quad (8)$$

which implies:

$$\begin{aligned} f_{\text{cl}} &= f_{\text{drag}} \frac{v_{\text{rel}}}{v_{\text{cl}}} \\ &= -\frac{1}{2} C_d A \rho_{\text{hot}} v_{\text{rel}}^2 \frac{|v_{\text{rel}}|}{v_{\text{cl}}} \\ &= -\frac{1}{2} C_d A \rho_{\text{hot}} \frac{|v_{\text{rel}}|^3}{v_{\text{cl}}}. \end{aligned} \quad (9)$$

Eq. (9) recovers the exact solution when the gas parcel is at rest (which is the typical case of heating of a hydrostatic gas) and when there is no relative velocity between the gas and the clump (i.e. no drag).

Physically, the drag forces always act to decrease the radial and tangential components of the velocity of clumps. While the radial velocity is replenished by the gravitational force, the tangential velocity monotonically decreases in time, so clumps lose angular momentum, becoming more radial in their trajectories. Since the angular momentum of the clump shells in our simulations is conserved, the clumps in the simulations cannot spiral towards the centre. To compensate for this problem, and allow clumps to reach the central core, a much smaller angular momentum is assigned to the clumps, placing them on almost radial trajectories.

¹ an algebraic scheme is such that the exact energy term is always added to one component and subtracted from the other explicitly, making sure the energy is conserved to the machine accuracy

2.1.3 Fragmentation of Clumps

Once the framework for accelerations and heating is defined, we proceed to implement recipes for clump evolution. In this work, we implemented only the most crucial additional recipes from DB08: clump fragmentation, and clump destruction. A clump fragments into n_{frag} clumps (2 thorough out this work) once it has repelled its own mass of ambient gas. The amount of gas repelled is calculated by numerically integrating over $\pi r_{\text{cl}}^2 \rho_{\text{gas}} v_{\text{rel}} dt$ in the same Runge-Kutta scheme used for the dark matter. After each timestep, the column mass and clump mass is compared. When the column mass exceeds m_{cl} , m_{cl} is divided by n_{frag} , n_{cl} is multiplied by n_{frag} , and the column mass integral is reset to 0. As m_{cl} becomes exceedingly small, its drag deceleration become large, and the periods between consequent fragmentation events become shorter. Clumps are destroyed when their mass decreases below a critical mass, at which conduction and evaporation is expected to disintegrate them completely (in this work - $10^4 M_{\odot}$).

2.1.4 Destruction of Clumps

The destruction of clump is achieved by adding its mass, to the corresponding baryonic shell. The velocity and angular momentum are not changed, and the internal energy and temperature is calculated by mixing the cold and hot components according to energy conservation by solving for the final internal energy, E_{int}^f in:

$$\begin{aligned} M(E_{\text{int}} + E_{\text{kin}} + E_{\text{grav}}) + m(e_{\text{int}} + e_{\text{kin}} + e_{\text{grav}}) = \\ (M + m)(E_{\text{kin}} + E_{\text{grav}}) + (M + m)E_{\text{int}}^f. \end{aligned} \quad (10)$$

with M, E correspond to the baryonic shell values, m, e to the clump shell. All energies are specific energies (per unit mass) and $e_{\text{int}} = C_v T_{\text{cl}}$ with $T_{\text{cl}} = 10^4 K$. Rarely, the final temperature will drop below $10^4 K$, at which case the final temperature is set to $10^4 K$. This is found to occur only for baryonic shells that are cold (around $2 \times 10^4 K$) and on a free fall to the BCG, and the temperature floor that is artificially applied never stops their infall. In this case, the fictitious energy is tracked throughout the run and is always negligible. The overall accreted mass is not effected by this correction.

2.1.5 Applicability to 3D Simulations

In the 1D case described above, the gas parcel is a finite-dimension gas shell, and the clump is a thin shell. A generalization for the 3D case is readily available, both for SPH and grid-based (Eulerian or Lagrangian) simulations that model dark matter as N-body particles: assign clumps to a dark matter particle according to eq. (2), calculate its acceleration according to eq. (9) and heat the gas according to eq. (7). In cosmological simulations, it is also necessary to self-consistently create those clumps. These can either be created semi-analytically according to cooling instabilities (Field 1965; Binney et al. 2009) or by identifying unresolved gaseous clouds and replacing them with clump particles (Kereš & Hernquist 2009, identify clump formation

on Milky Way scales, but resolution would not allow to scale this procedure to galaxy cluster scales).

2.2 Cell splitting - a 1D Adaptive Mesh Refinement

In the Lagrangian formalism, the amount of baryonic mass within each shell is constant throughout a simulation. Clump destruction, however, violates that by dumping mass into the baryonic shells at the event of clump destruction. This mass deposition is expected to occur preferentially at specific regions. Indeed, the simulations discussed below initially caused the formation of a few extremely massive shells that absorbed most of the mass of the clumps. This situation (of large contrasts between adjacent shells in mass and widths) reduces the accuracy of the numerical scheme, and effects the accretion rates onto the BCG. To overcome this, an adaptive splitting of baryonic shells is performed: when the shell is wider by some factor than both its neighbours, or when the shell's width divided by its radius exceeds some preset fraction, the shell is split to two. The factors ultimately used were: $\Delta r_n > 4 \times \max(\Delta r_{n-1}, \Delta r_{n+1})$ and $\Delta r_n/r_n > 0.2$ (with Δr_n and r_n the width, and central radius of shell n) which caused splitting to occur a few dozens of times throughout a full, Hubble time simulation.

A shell is split into two constant mass shells. Values that are naturally defined at centres of shells (density, temperature) are treated as step functions and their values are equal in the two new shells. Values that are defined on boundaries (radius, velocity, angular momentum) are interpolated linearly with mass. This definition ensures that the total internal energy of the system remains the same. The potential and kinetic energies, however, can change. This energy non-conservation is not corrected for explicitly. Rather, it is treated as non-conservation and tracked throughout the run. In the high resolution simulations shown below, the total, overall energy is conserved to better than 10^{-2} over a Hubble time.

2.3 Convection and Mixing Length Theories

2.3.1 Convection

A long term balance between cooling and heating requires, in addition to sufficiently large energy injection, a correct distribution of this energy. The cooling rate, at constant pressure, scales as $\dot{e}_{\text{cool}} \sim \rho^{1.5}$, and most heating mechanisms (the drag forces discussed here, dynamical friction, radiative heating from supernovae and AGNs) generally heat according to $\dot{e}_{\text{heat}} \sim \rho$. Even if at some point in space, and at some initial time, $\dot{e}_{\text{cool}}/\dot{e}_{\text{heat}} = 1$, this ratio scales like $\rho^{0.5}$. This relation indicates a positive feedback so if density increases, cooling is more efficient, causing a further increase in density at constant pressure, and unstable cooling will occur. Vice versa, a density decrease increases the relative importance of heating over cooling, decreasing the density further, and an over-heating instability occurs. This point has been made by Conroy & Ostriker (2008),

using 1D hydrodynamic calculations of clusters initially hydrostatic within a static potential well. They find that stable, long term equilibrium requires fine tuning of the heating efficiency which is unlikely. The present work differs in that it treats the gravitational drag feedback and the cluster evolution from initial cosmological perturbation consistently, but should still suffer from a heating instability. Such an overheating will manifest as a shell or region of shells of gas continuously becoming hotter and under-dense, with very high entropy. In a 3D configuration, this entropy inversion is unstable to convection when entropy is declining outwards: a slightly under-dense parcel of gas floats buoyantly, carrying energy and momentum outwards, and over-dense parts sink towards the centre reducing the average entropy and specific energy of the core. For our 1D simulation we invoke a 1D subgrid model for convection - mixing length theory (Spiegel 1963).

2.3.2 Mixing Length Theory

Convection occurs when an adiabatic displacement of a parcel of gas, in pressure equilibrium with its new position, results in a net force on that parcel tending to increase the displacement. This requires that, for an upward displacement, the temperature of the gas parcel will be smaller than its surrounding:

$$\begin{aligned} \Delta \nabla T &\equiv \left(\frac{\partial T}{\partial r} \right) - \left(\frac{\partial T}{\partial r} \right)_s \\ &= \left[\left(\frac{\partial T}{\partial S} \right)_P \frac{\partial S}{\partial r} + \left(\frac{\partial T}{\partial P} \right)_S \frac{\partial P}{\partial r} \right] - \left(\frac{\partial T}{\partial P} \right)_S \frac{\partial P}{\partial r} \\ &= \left(\frac{\partial T}{\partial S} \right)_P \frac{\partial S}{\partial r}, \end{aligned} \quad (11)$$

with the first term in the r.h.s corresponding to the actual temperature derivative in the profile, and the second to the adiabatic change in temperature as a result of the pressure profile of the halo. A negative value of $\Delta \nabla T$ allows for convection to occur. It is convenient to derive this relation using a form of the ideal equation of state in which the two thermodynamic free parameters are the entropy, S , and the pressure, P .

$$\begin{aligned} P &= \frac{N_A k_B}{\mu} \rho T, \\ S &= \frac{N_A k_B}{\mu} \ln \frac{T^{3/2}}{\rho}, \end{aligned} \quad (12)$$

can be inverted (setting $\hat{\mu} = N_A k_B / \mu$) into:

$$\begin{aligned} \rho &= (\hat{\mu} P)^{3/5} e^{-2/5\hat{\mu} S}, \\ T &= (\hat{\mu} P)^{2/5} e^{2/5\hat{\mu} S}. \end{aligned} \quad (13)$$

Plugging these relation into the derivatives in eq. (11) we get:

$$\Delta \nabla T = \frac{2}{5} \hat{\mu} T \frac{\partial S}{\partial r}, \quad (14)$$

recovering the known results that when the composition of the gas is constant, entropy inversion leads to convection.

The buoyant bubbles rise for a typical length before being destroyed by Kelvin Helmholtz instability or conduction. The details of this destruction depend on the size of the bubbles, the smoothness of the density and gravitational profile, conduction and magnetic fields. Solving for it requires fine 3D simulation of the convective process. We replace this dependency by a free dimensionless parameter, the mixing length (L), assuming that bubbles rise a distance, H_P , which is proportional to the atmospheric scale length of the halo at each point:

$$H_P = L \frac{P}{\rho g}, \quad (15)$$

with $g = GM/r^2$. A typical acceleration is:

$$a = g \frac{\delta \rho}{\rho} = g \left(\frac{\partial \rho}{\partial S} \right)_P \frac{\partial S}{\partial r} H_P, \quad (16)$$

so a typical bubble velocity is:

$$v = (2a H_P)^{1/2} = H_P \left[2 \frac{g}{\rho} \left(\frac{\partial \rho}{\partial S} \right)_P \frac{\partial S}{\partial r} \right]^{1/2}. \quad (17)$$

Once the velocity exceeds the local sound of speed in the halo shocks are created which quickly act to mix the bubble with its surrounding. In the following calculation the velocity is not allowed to exceed the speed of sound, c_s , and in that case H_P is reduced until $v = c_s$ in eq. (17). A **maximal convection** model is a model with arbitrary high L , so effectively the bubbles always accelerate until the speed of sound, at which time they are broken and mixed.

The Flux of energy per unit surface per unit mass is:

$$F_c = C_P v [\Delta \nabla T H_P] = C_P v \left[\frac{2}{5} \hat{\mu} T \frac{\partial S}{\partial r} H_P \right], \quad (18)$$

which is determined by the halo profile from the simulation at each time, and the mixing length L . C_P is the constant pressure heat capacity and is related to $\hat{\mu}$ by $C_P = 5/(2\hat{\mu})$.

A numerical solution of the mixing length model requires evaluation of the incoming and outgoing fluxes from the boundaries of each radial shell. The fluxes depend on the temperature gradient between each shell and the ones directly below and above it, and interpolation of thermodynamic properties from the shell centres to the shell's edges is required. A solution using an explicit numerical scheme (with the fluxes determined at the beginning of each timestep) requires extremely small timesteps to avoid negative temperatures, so an implicit scheme which solves simultaneously for all the temperatures and fluxes at the end of each timestep in each convective area was implemented. This is done by inversion of the three-diagonal matrix which is obtained by discretization of eq. (18).

In the context of the clump heating discussed in this paper, it should be emphasized that the convection is not between the cold gas in the clumps and the hot surrounding. It is only within the hot component, and is the result of heating and cooling of that component. The convection model assumes linear perturbations within a

single gas phase which separates into two phases (hot buoyant bubbles, and cold sinking gas). The propagation of clumps, which have a typical over-densities of $\gtrsim 1000$ is followed explicitly using the processes described in §2.1.2 - §2.1.4.

The ICM is mildly magnetized, with the non-thermal magnetic pressure contributing at most 10% of the total pressure (Churazov et al. 2008). This effect could lead to heat-flux buoyant instability (HBI; Parrish et al. 2009) even when the entropy profile is monotonically increasing provided there is a temperature inversion near the core ($dT/dr > 0$). These instabilities act to align the magnetic fields perpendicular to the temperature gradient, in a manner that suppresses further conduction (Parrish et al. 2009). Convective motions are also somewhat suppressed even for material that is hydrodynamically convectively unstable ($ds/dr < 0$). The specific strength of this suppression in this particular case is left for future works.

2.4 The Observed Properties of Hot Gas with Cold Clumps

In the current implementation, when clumps are destroyed, their mass is added to the hot component instantly. In reality, the process of KH fragmentation, followed by small scale evaporation and conduction of the debris will yield a multiphased gas, with an effective entropy and temperature which is between the values of the hot and cold phases. As will be shown later (§4), the clump density and clump destruction rate increase towards the centre so effective cooler and lower entropy values are expected there. The radiative signature of gas heating through all the temperatures between $10^4 K$ to the cluster ambient gas temperature of $\sim 3 \times 10^7 K$ is expected to be significantly different from that of radiative cooling since it is governed by heating processes (emission spectrum from heating gas, albeit by other heating mechanisms have been studies in Voit & Donahue 1997; Oh 2004). A framework of heating and cooling processes in layers between hot and cold media have been proposed by Begelman & Fabian (1990); Gnat et al. (2010).

The observational signature of clump break up would require detailed 3D simulation of clump interactions with cluster core gas, and multiphased modeling of the radiative signature during the heating process, and is beyond the scope of this work. Instead, we will plot below the mass weighted entropy and temperature of the two components. This is a lower limit for the observed entropy and temperature as the clumps' contribution to the luminosity, particularly at X-ray wavelength, is probably small. Physically, it corresponds to the thermodynamic properties expected in the event of full mixing between the cold and hot phase.

3 RESULTS

The simplified model described in §2 spans a multidimensional parameter space including the fraction of accreted gas in clumps, the initial clump masses, the num-

ber of fragments that a clump breaks up to, and the mixing-length parameter for convection. In the absence of additional physical insight concerning the formation mechanism and properties of these clumps, we attempt to find a working set of values for the model parameters, to serve as a feasibility test and hopefully provide clues for acceptable values of the key parameters. Ultimately, a more systematic survey of parameter space will have to be conducted, with physically motivated values for key parameters such as number and mass of clumps.

In this section we restrict ourselves to one typical CC cluster halo with virial mass of $3 \times 10^{14} M_\odot$ by $z = 0$, a diffuse baryon fraction of 10%, and a smooth accretion history according to the average growth rate of the main progenitor a la Neistein et al. (2006) (see Birnboim et al. 2007, for a detailed description). The metallicity is assumed to be constant at $Z = 0.3 Z_\odot$, and the cooling is Bremsstrahlung and line cooling according to Sutherland & Dopita (1993). The initial resolution is 2000 baryonic shells and 10,000 dark-matter shells, roughly logarithmically spaced in their initial radii. When shells expand, the adaptive mesh refinement algorithm splits them (§2.2), so the resolution near the cluster core (~ 50 kpc) at all times is better than ~ 2 kpc. This yields converged results in terms of the profiles and the amount of gas that cools. We implement three different models for clump heating, as follows:

(i) Model C is the null model with no clump heating and no convection. It is meant to reproduce the over-cooling problem.

(ii) Model CH adds clump heating but no convection, so it should show the over-heating instability. The fraction of baryons in clumps is 5% and the clump initial mass is $10^8 M_\odot$. The clumps are simulated by 10,000 clump shells (§2.1.2).

(iii) Model CHC has the same clump heating as in CH but with maximum convection turned on (§2.3.2). The smoothing by convection is supposed to regulate the clump heating and yield relaxed clusters compatible with observations.

Figure 1 shows the time evolution of the gas in our simulated cluster comparing the three different models for cooling, clump heating and convection. The initial Hubble expansion and consequent turnaround of the Lagrangian gas shells is clearly seen, and the virial shock can be easily identified after a collapse by a factor of ~ 2 , both by jump in temperature from below $10^4 K$ to above $10^7 K$, and by the abrupt slow down of the infall velocity, which is almost brought to a halt behind the shock. The global large-scale properties of the cluster are not affected by the addition of heating and convection. The virial radius evolves in a similar way, and the typical temperature in the halo at $z = 0$ remains at $T \sim 2 - 3 \times 10^7 K$ ($\sim 2 - 3$ keV), consistent with the expected virial temperature of $2.2 \times 10^7 K$ for a cluster of virial mass $3 \times 10^{14} M_\odot$. However, the models differ at the core, within the innermost 100 kpc especially during the last 6 Gyr of evolution. Model C shows inward cooling flows at all times, as expected (Fabian 1994). With the addition of clump heating in Model CH The cooling flows are stopped before $t = -6$ Gyr, the

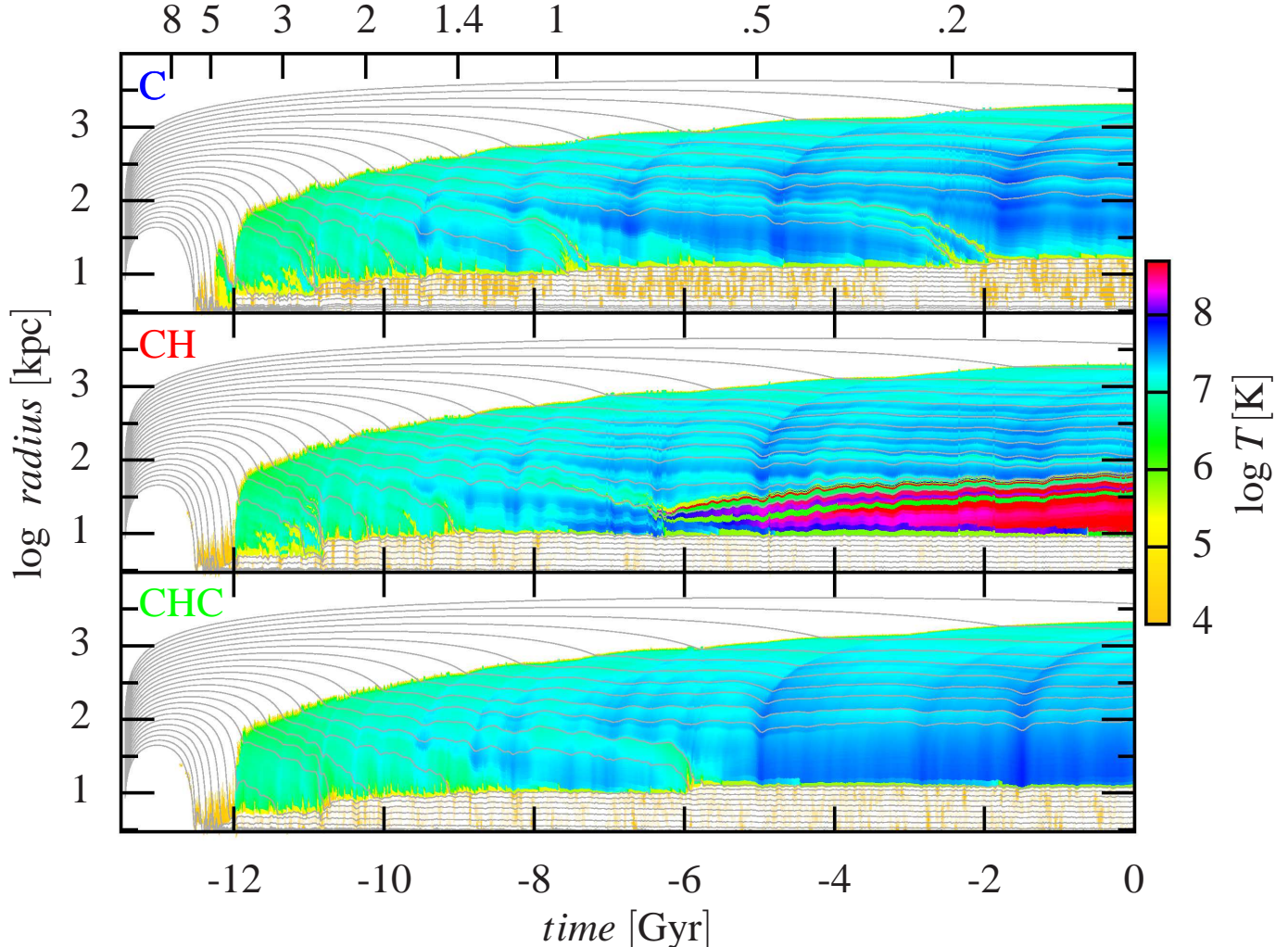


Figure 1. The time evolution of the gas in a cluster for the three different models of clump heating. Shown in grey lines are the evolving radii of 25 spheres that encompass fixed baryon masses equally log-spaced in the range $10^{10} - 5 \times 10^{13} M_{\odot}$. The dark matter and clumps are not shown. The final halo mass is $3 \times 10^{14} M_{\odot}$. Look-back time and redshift are marked at the bottom and at the top. The color refers to gas temperature. Top: Model C, cooling only. Middle: Model CH, cooling and heating. Bottom: Model CHC, cooling, heating and convection. Model C shows cooling flows in the core between 10 and 100 kpc during the last 6 Gyr. Model CH shows core over-heating and expansion in the last 6 Gyr, and Model CHC demonstrates how convection regulates the heating and brings the cluster to an equilibrium.

gas in certain shells is over-heated to extreme temperatures $\gtrsim 10^8$ K, these shells are interlaced with cooler shells of $\sim 10^6$ K, and together the whole core inflates. This behavior is in conflict with the relaxed nature and smooth entropy and temperature profiles of CC clusters (Donahue et al. 2006). The addition of convection in Model CHC removes the over-heating, and keeps the core in equilibrium at the virial temperature with no cooling flow. A more detailed comparison of the models and observations follows.

3.1 Time Evolution of X-ray Luminosities and BCG Masses

Figure 2 shows the evolution of X-ray luminosity, the mass of the BCG, and the accretion rate onto it, for the three different models. The BCG is represented by the mass in the “disc”, the mass that is supported by

angular momentum in the 1D simulations, extending to ~ 10 kpc. The X-ray luminosity is obtained as the total cooling radiation from the gas outside the BCG². The quantities are smoothed over 1 Gyr to erase sharp features that result from the discreteness of the calculation in the idealized spherical calculation.

Model C shows a variable luminosity, which occasionally exceeds by an order of magnitude or more the observed luminosity of $10^{44} - 10^{45}$ erg sec⁻¹ as derived from the $L_x - T$ relation (Edge et al. 1990; David et al. 1993; Markevitch 1998). In Model C the final BCG mass exceeds $2 \times 10^{12} M_{\odot}$ and the accretion rate, which is an indicator for the star formation rate, has long episodes

² Most of the energy is emitted from cooling of \sim keV gas, and is predicted to contribute to the X-ray luminosity that is relevant to the $L_x - T$ relation (for example: Markevitch 1998).

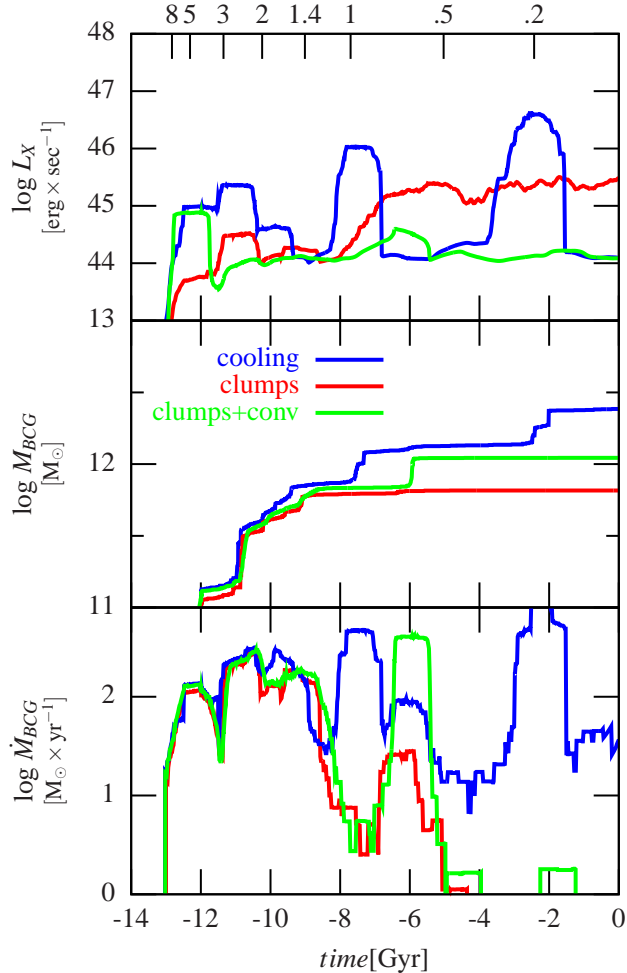


Figure 2. Time evolution of X-ray luminosity (top), BCG mass (middle), and BCG accretion rate (bottom), all smoothed over 1 Gyr.

where it is in the range $100-1000 M_\odot \text{yr}^{-1}$, at odds with observed CC clusters. When clump heating is added in Model CH, the cooling flow into the BCG is drastically suppressed since before $t \sim -8$ Gyr, and it reaches a complete shutdown after $t \sim -5$ Gyr. The luminosity maintains a high level of $\sim 2 \times 10^{45} \text{ erg sec}^{-1}$ since $t \sim -7$ Gyr. This results from the over-heating instability in the halo core, leading to very dense shells that boost the dissipation due to drag interaction with the clumps and enhance the resulting radiation. The addition of convection in Model CHC brings the BCG mass to a constant value of $\sim 10^{12} M_\odot$ with no detectable cooling flow since $t \sim -6$ Gyr. The smoothing of the instability brings the luminosity to a low value of $\sim 10^{44} \text{ erg sec}^{-1}$, consistent with the observed $L_X - T$ relation.

3.2 Entropy and Temperature Profiles

The $z = 0$ entropy profiles of the three models are plotted in Fig. 3 and the temperature profile of model CHC is plotted in Fig. 4. The entropy profiles in the outer halo, overall increasing close to linearly with radius and

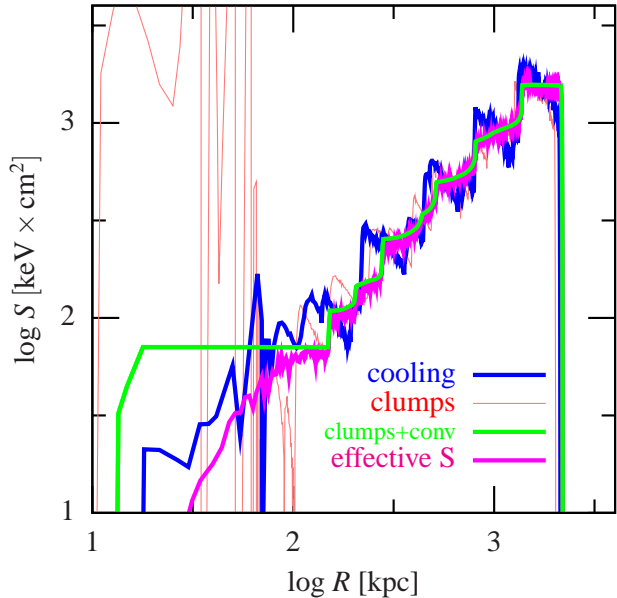


Figure 3. Radial profiles of entropy at $z = 0$ for models C, CH and CHC. Shown in three curves is the entropy of the hot medium, and an additional curve marked CHC_{eff} refers to the effective entropy of the mixture of hot gas and the surviving cold clumps, computed as a mass-weighted average.

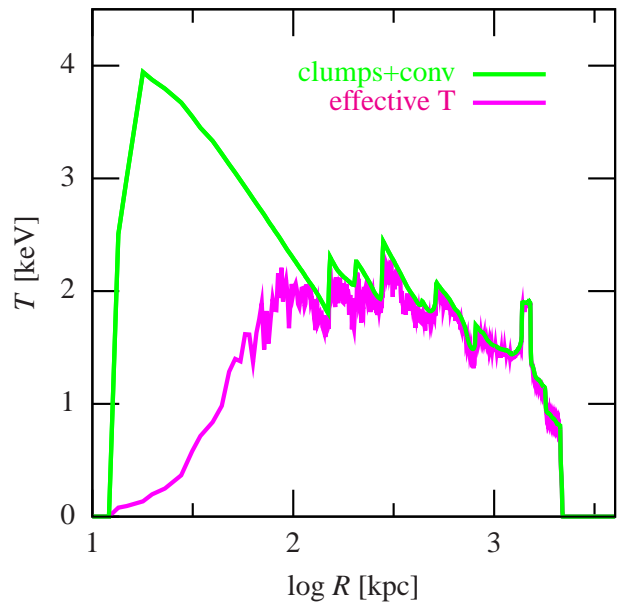


Figure 4. Radial profiles of temperature at $z = 0$ for model CHC, for the hot medium and for the mixture of hot medium and cold clumps, computed as a mass-weighted average.

having values $\sim 100 \text{ keV} \times \text{cm}^2$ at 100 kpc, are similar in all models and consistent with observations of CC clusters (Donahue et al. 2006; Cavagnolo et al. 2009). The apparent periodic fluctuations represent cold fronts that result from mergers of outward-propagating shocks at regular intervals with the virial shock (also visible in Fig. 1), which have been studied in Birnboim et al.

(2010). While the fluctuations in Models C and CH are locally non-monotonic, the entropy profile of Model CHC is monotonically increasing throughout because the convection removes negative entropy gradients. Model CH shows a high-entropy core due to overheating, and a strong variability representing a mixture of cold-dense and hot-dilute shells that result from the overheating instability, both in conflict with observations. The convection introduced in Model CHC removes the fluctuations and produces what seems to be a flat core entropy profile inside 150 kpc at 50 keV \times cm 2 . Such a core is still inconsistent with CC cluster cores, but recall that the profile shown is limited to the entropy of the hot component alone. The effective entropy that could actually be observed is a mixture of the entropy in the hot gas, cold clumps, and anything in between as discussed in §2.4. The effective entropy profile shown in Fig. 3 is monotonically increasing in the core down to ~ 30 kpc, consistent with CC clusters.

The temperature profile of Model CHC at $z = 0$ is plotted in Fig. 4. It shows a roughly isothermal halo at the virial temperature outside the core of ~ 100 kpc, with a mild decline toward the virial radius, as observed (Donahue et al. 2006). This large-scale temperature profile has not been affected much by clump heating and convection. The temperature of the hot component is rising toward the centre, by a factor of ~ 2 , but the effective mass-weighted temperature of the mixture of hot and cold components is declining toward the centre, by a factor of a few. This mass-weighted effective temperature (that corresponds to the single temperature the gas would if the phases were fully mixed) is a lower limit to the luminosity-weighted temperatures observed, and is consistent with the moderate temperature decline in CC cluster cores. The temperature profiles of the various models, and its time evolution, can also be seen in Fig. 1.

4 OBSERVATIONAL SIGNATURES OF CLUMP HEATING

The model parameters chosen in this paper were motivated by the analysis of DB08 and were calibrated such that the model crudely reproduces the properties of CC clusters in order to demonstrate the feasibility of such a model of gravitational heating. The reproduced properties include the BCG mass, the cold mass accretion history, the X-ray luminosity and the entropy and temperature profiles. This model makes additional predictions that could distinguish it from other heating models such as the ones based on AGN feedback. Some of these predictions are discussed here.

4.1 Cold gas in the ICM

The mass function of clumps at every radius is a distinctive prediction. Assuming an initially uniform population of $10^8 M_\odot$ clumps, Fig. 5 shows the profiles of number density and average clump mass for Models CH and CHC. The fraction of volume occupied by cold clumps is shown in the bottom panel. These predictions depend

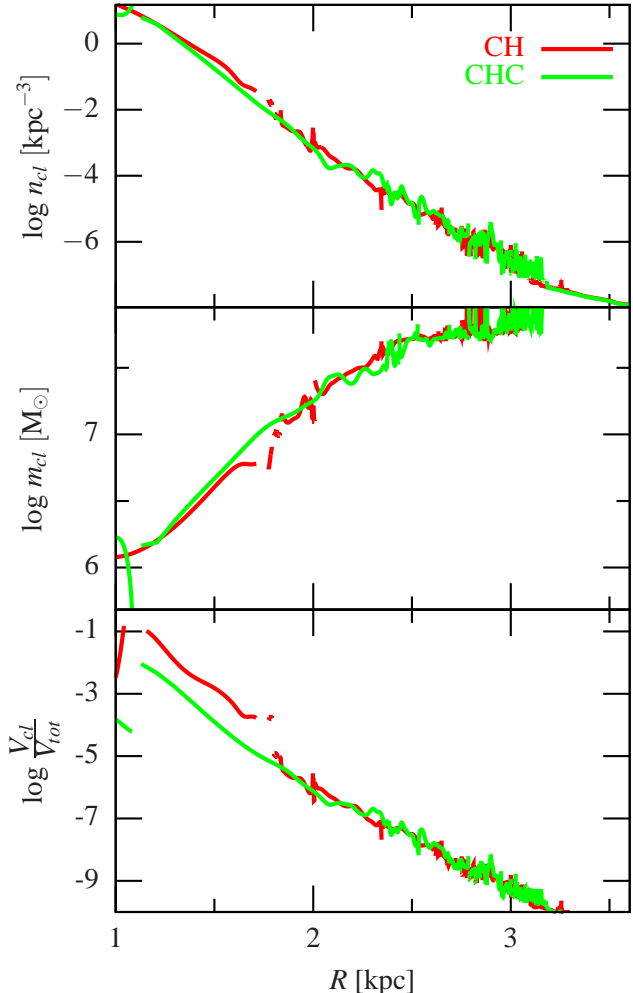


Figure 5. Average number density of clumps (top), average clump mass (middle) and fractional volume in clumps (bottom) as a function of radius at $z = 0$ for Models CH and CHC.

on the specific choice of the initial mass of the clumps and on the baryonic fraction of mass in these clumps. The number density of clumps increases toward the centre $\propto r^{-2}$, partly reflecting the general density profile of the cluster and partly because of the break up of clumps into fragments (§2.1). Once clumps are fully destroyed (fragments $< 10^4 M_\odot$), their mass is added to the hot component, and they are no longer plotted in Fig. 5. The figure thus shows the steady state population of clumps as they are continuously accreted and destroyed. The average clump mass is declining from the initial value of $10^8 M_\odot$ in the outer halo to $\sim 10^6 M_\odot$ near the centre, reflecting the clump fragmentation as they flow in. The fraction of volume occupied by the cold clumps peaks at a few percent near the cluster core, and it drops to smaller values at larger radii. This justifies ignoring the additional pressure caused by this component.

The clumps are initially cold, and, except for the mild compression they undergo as they fall in following the increasing pressure of the ambient gas, they

are not expected to heat up or emit much radiation. However, as the clumps are disrupted by hydrodynamical instabilities and possibly also by tidal effects, they fragment into smaller pieces for which conduction and evaporation become more important (§2.4). Once heated to intermediate temperatures, the gas begins to radiate. Spectroscopic observations could in principle constrain the validity of this model in comparison with AGN-feedback models, where one expects gas cooling rather than heating through the intermediate temperatures. The current simplified implementation of clump heating does not permit a proper comparison, which is left for future work. Additionally, three-dimensional simulations are required for a detailed analysis of the shape of the clumps as they are stretched and destroyed perhaps leading to morphologies resembling filaments (Murray & Lin 2004). This emission, in H_{α} and line and continuum emission of the intermittent X-ray temperature gas, may allow more accurate comparisons of this model with the observed profiles in cluster cores. Observations in the Perseus cluster (NGC 1275) (Conselice et al. 2001; Fabian et al. 2008) show a complicated structure of H_{α} filaments and blobs. The typical masses of these features are $10^6 - 10^8 M_{\odot}$, consistent with the allowed mass range for clumps in DB08, and with the distribution predicted by our model (Fig. 5). We note that this result depends on the initial mass of the clumps - a free parameter here. The consistency of this prediction with observation is an indication that our choice of initial mass of $10^8 M_{\odot}$ is reasonable. Fabian et al. (2008) invoked strong magnetic fields to stabilize the filaments for cosmological times, such that their age can match that of the observed radio bubbles. Our heating model suggests instead that these filaments are constantly being destroyed, as new clumps enter the cluster core, get stretched and destroyed, and create new filaments. The projected filling factor of these structures approaches unity within the innermost 10 kpc and it drops outwards (Conselice et al. 2001). Such a behaviour is predicted by our model (Fig. 5). H_{α} emission in other clusters have been reported by Heckman et al. (1989), who found that the cold gas has velocities at random directions rather than a coherent radial cooling-flow pattern. This kinematics could be interpreted as clumps oscillating in and out at the vicinity of the BCG. Structures of neutral gas are also seen in the Virgo Cluster by the ALFALFA 21cm survey (Giovanelli et al. 2007; Kent et al. 2007) showing evidence for neutral gas arranged in clumps, with masses as low as the detection limit of $2 \times 10^7 M_{\odot}$, sometimes with no optical counterparts.

4.2 Turbulence in the ICM

Another prediction of this model is the power of turbulence that is produced in the ICM. When the clump velocities are subsonic with respect to the ICM, the energy and momentum of the drag are first converted to kinetic energy in turbulence, which cascades down to smaller scalelengths where it dissipates into heat. When the motion is supersonic, some of the energy is converted directly into heat, but since momentum is con-

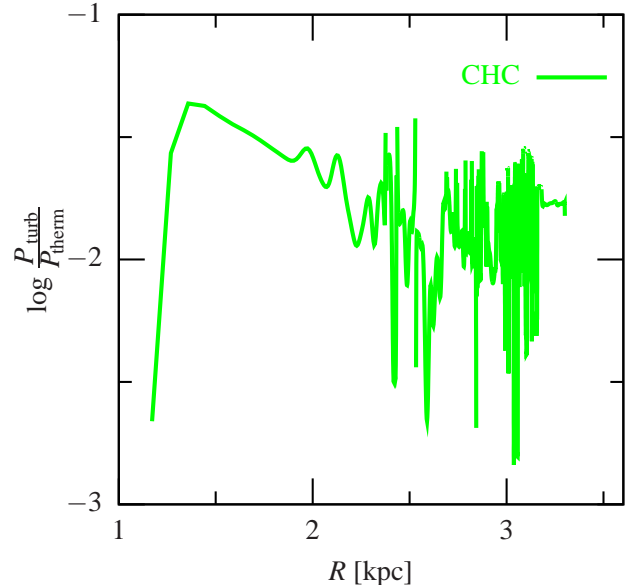


Figure 6. Ratio of turbulent pressure to thermal pressure as a function of radius at $z = 0$ for Model CHC.

served, some of the energy must be transferred as kinetic energy to the ICM. We assume that the turbulence is generated on a scalelength comparable to the average distance between clumps, L , and that a Kolmogorov spectrum governs the cascade of eddies from this scale to smaller scales. The turbulent energy and pressure are then

$$e_{\text{turb}} = \frac{3}{2} c_0 (\dot{e}_{\text{drag}} L)^{2/3}, \quad (19)$$

$$P_{\text{turb}} = (\gamma - 1) \rho_{\text{ICM}} e_{\text{turb}} = c_0 \rho_{\text{ICM}} (\dot{e}_{\text{drag}} L)^{2/3},$$

(Landau & Lifshitz 1959), with $c_0 = 2.1$ taken from Popo (2000). The amplitude of the turbulence spectrum, and the turbulent pressure can thus be determined once we know the average distance between clumps and the drag heating rate at every radius. The ratio between the turbulent pressure and the thermal pressure for Model CHC is plotted in Fig. 6. The level of turbulent pressure in the cluster core is at the level of $\sim 6\%$ of the thermal pressure, in qualitative agreement with observations (Rebusco et al. 2006; Churazov et al. 2008).

4.3 High Velocity Clouds in the Galactic Halo

High velocity clouds (HVCs) are observed in 21cm HI data (Blitz et al. 1999) as concentrations of gas moving at velocities $> 100 \text{ km s}^{-1}$ relative to the rotating frame of the Milky Way. Options for the spatial origin of the HVCs range from the Milky Way (MW) disc (Wakker et al. 2008, and references therein), through the Magellanic clouds (Olano 2008), to extragalactic origin (Blitz et al. 1999). The distance to and the ionization fraction of individual clouds (and therefore their size and mass) are unknown. Putman et al. (2003) estimated distances of HVCs based on their H_{α} flux and models for the emission of ionizing radiation from the

MW. They find, within the modeling and measurement uncertainties, that most HVCs are within a distance of $\lesssim 30$ kpc, indicating a mass range of $10^4 - 10^8 M_\odot$, (Putman et al. 2003; Birnboim & Loeb 2009). Other estimates by absorption features (Thom et al. 2008) yield comparable distances and masses. The origin of the HVCs is unclear. Models have proposed that they form within the Galactic halo by cooling instabilities (Maller & Bullock 2004; Kereš & Hernquist 2009). See, however, Fraternali & Binney (2008). Binney et al. (2009) analyzed formation of clumps in smooth MW halo conditions from thermal instability and concluded that it is unlikely to occur near the centre. They find, however, that the conditions become favorable closer to the halo virial radius and when the entropy profile is shallow (as is shown numerically in Kaufmann et al. 2009). Their stability analysis tests growth of instability from infinitesimal perturbations but the growth of non-linear perturbations caused by shocks, collisions, and gravitational perturbers depends on initial conditions. The line-emission peak of the cooling curve at $\sim 10^5 K$ would make the warm cosmic filaments outside clusters more susceptible for clump formation. However, clumps have been shown to be a natural consequence of cold-flow filament breakup by hydrodynamic instabilities (Kereš & Hernquist 2009). For example, streams that do not flow radially to the halo centre are susceptible to Rayleigh-Taylor instability. Also, shocks that originate from the galaxy, e.g., by mergers or by starbusts, are likely to form clumps by Richtmyer-Meshkov instability. The destruction of these clumps, and their interaction with the Galaxy and the IGM, are likewise under debate (Fraternali & Binney 2008; Kereš & Hernquist 2009).

We point at an obvious analogy between the observed Galactic HVCs and the clumps addressed in this paper. Their masses are comparable, and their spatial distributions in the halo and toward its centre are possibly similar. The larger pressure in the ICM of a more massive halo would make the cluster clumps denser than the Galactic HVCs (by the ratio of virial temperatures which is more than 10 times larger for clusters), so clumps of a similar mass could survive longer in clusters, allowing them to travel to the centre according to the estimates in §2. The total mass encompassed in HVCs seems to be $\gtrsim 10^9 M_\odot$, making it a few percent of the total baryons in the MW halo, in good agreement with our fiducial choice of parameters. A missing piece of the model is the yet unspecified origin of the clumps, in terms of physical mechanism and location. The existence of HVCs provides circumstantial evidence that such clumps might form. As long as the clumps are formed before they fall into the halo, or even if they form inside the halo at a radius that is not much smaller than the virial radius (Maller & Bullock 2004; Kereš & Hernquist 2009), the gravitational energy that is released during their infall is significantly larger than the energy required for heating the clumps to the virial temperature (DB08).

5 DISCUSSION AND CONCLUSION

The concept of gravitational heating of ICM gas as a partial or full solution to the cooling-flow problem is more general than the specific clump model discussed in this paper. The gravitational energy that is released as baryonic matter falls in through the halo potential well is enough to balance the cooling rates in groups within haloes of virial masses $\sim 10^{13} M_\odot$, and it exceeds the cooling rate by more than an order of magnitude in cluster haloes $\sim 10^{14-15} M_\odot$ (DB08). This point has also been made in Fabian (2003); Wang & Abel (2008); Khochfar & Ostriker (2008). El-Zant et al. (2004) and Faltenbacher & Mathews (2007) tap into the same energy source, but utilize dynamical friction that is less effective. Naab et al. (2007); Johansson et al. (2009) show, however, that dynamical friction can efficiently stop gas accretion onto massive elliptical galaxies. Conduction also taps into this energy source, and was proposed three decades ago (Bertschinger & Meiksin 1986; Rosner & Tucker 1989). It is probably ruled out because of magnetic field suppression of the conduction (Binney & Cowie 1981; Fabian 1994, and reference within), and because the resulting profiles would have a flat temperature core (Bregman & David 1988). See, however, Narayan & Medvedev (2001) and Kim & Narayan (2003).

The challenge for every heating model is to distribute the energy uniformly throughout the cluster core both in space and time (De Young et al. 2008; Cattaneo et al. 2009). In order to obey the observational constraints, the heating mechanism should suppress the gas mass that actually cools by two orders of magnitude. Such a shutdown requires that the mechanism should act smoothly over a scale of a few kpc, set by the smallest object that would cool in the absence of feedback while being continuously heated by conduction from its surrounding. This scale follows from

$$L_{\text{cond}} \sim \sqrt{\eta \kappa_{\text{Sp}} t} = 7 \sqrt{\eta_{0.2} T_2^{5/2} n_{-2}^{-1} t_8} \text{ kpc} \quad (20)$$

with κ_{Sp} the Spitzer coefficient (Spitzer 1962), η the reduction of the Spitzer coefficient due to magnetic fields, t the cooling time of the gas, and $T_2 = kT/2 \text{ keV}$, $n_{-2} = n/10^{-2} \text{ cm}^{-3}$, $t_8 = t/10^8 \text{ yr}$, $\eta_{0.2} = \eta/0.2$. The value $\eta = 0.2$ is a reasonable upper limit for the efficiency of conduction (Narayan & Medvedev 2001). It also has to be temporally smooth over the cooling timescale, which is a few 10^8 yr at most (Donahue et al. 2006). The fact that the energy source of gravitational infall is automatically distributed over the cluster volume and over Hubble times makes it easier to meet this challenge with gravitational heating than it is with AGN-feedback models, where the source is on scales ten orders of magnitude smaller than the cluster scales. However, the coupling of the infalling baryons with the ICM should be such that most of the gravitational energy is deposited in the cluster core.

This paper addresses one specific scenario of gravitational heating, in which the mechanism for feeding the energy into the ambient ICM is via hydrodynamic drag acting on small clumps of cold gas. In a typical cluster, with a modest gas fraction of $\sim 5\%$ of the ac-

creted baryons in cold clumps of $\sim 10^8 M_\odot$, the clump heating suppresses the cooling flows toward the BCG for the last 6 Gyr. The conditions at the core do not affect the incoming clumps, so the process is not strictly self-regulating. Regardless, we find that the large-scale properties of the cluster, such as the overall gas fraction, virial shock and temperature outside the core, are unaffected by the heating. Furthermore, the core does not explode; it reacts to the heating smoothly and quiescently without a need for inherent self regulation. Due to the over-heating, the central density decreases and the total X-ray luminosity emitted from the core (Fig. 2) declines such that the core obeys the observed $L_x - T$ relation. On cluster core scales, convection acts to flatten the entropy profile of the hot component and carry heat outwards as expected. The effective entropy profile after taking into account the cold clumps as well does not exhibit an entropy core, and is consistent with observed entropy profiles, to within the model limitations that are discussed. A local instability caused by the linear dependence of the heating rate on density ($\dot{e}_{\text{heat}} \sim \rho$) acts to create extreme entropy and temperature peaks of sub-kpc scales. These peaks create strong convection that, once accounted for in the simulations, stabilize the heating process on local scales as well.

With the fiducial values of the parameters used in this work in a $3 \times 10^{14} M_\odot$ cluster halo, the model is successful in quenching the cooling flows and in reproducing adequate BCGs, X-ray luminosities, and entropy and temperature profiles. The model also predicts the expected level of turbulence in clusters, and the fraction of cold gas as a function of radius. These two observables, the turbulence level and cold gas fraction and morphology, were not deliberately fitted here, and are a prediction of this model. They are not naturally constraint by most AGN models.

In DB08 we analyzed clump heating in a static halo using a Monte-Carlo approach to simulate an ensemble of clump trajectories. We realized that the heating rate in the core is higher than the cooling rate, which could cause the core to expand. In order to see how the cluster could reach a steady-state configuration one must allow the system to respond dynamically. The current implementation of the model using a 1D hydro code to simulate a cluster in the cosmological context allows us to do just that. We find that convection can regulate the over-heating instability and produce a cluster with no cooling flow in steady state. The net effect of the dynamical response is to make the heating more efficient. For example, with 5% of the baryons in $10^8 M_\odot$ clumps inflowing into a static $3 \times 10^{14} M_\odot$ cluster, our estimates in DB08 indicates a heating to cooling ratio slightly below unity, while here we find a stronger effect, predominantly due to the net expansion of the core. The dynamical evolution of the cluster (Fig. 1) is noticeable especially from $z \sim 2$ and on, as the core takes a different thermodynamic trajectory in response to the heating. The BCG mass is smaller, and the core density is lower than in the simulation without heating. It is therefore possible that other heating mechanisms that were tested within a static framework (Conroy & Ostriker 2008; Fabian 2003; Kim & Narayan

2003; Kim et al. 2005; Ciotti & Ostriker 2007) would also show different evolution tracks once the gas is allowed to dynamically adjust to the energy input while the halo is growing.

The main missing piece in the proposed model of clumps as the agents for depositing the gravitational energy of infall in the ICM core is the unspecified mechanism and birthplace for the formation of clumps with the desired properties of frequency and mass. While clumps probably do not form in-situ at the cores of clusters (Binney et al. 2009), they can form within cosmic filaments and on the edges of haloes. Non-linear perturbations and complicated halo geometries can stimulate the formation of such clumps (Kereš & Hernquist 2009). The analogy between the observed HVCs and the desired clumps for heating clusters is promising and may provide a clue for the origin of these clumps.

The degree of clumpiness needed for effective clump heating, at the level of $\sim 5\%$, does not seem to be very demanding. The clumps may be hard to detect outside the halo virial radius as their temperatures are expected to be only slightly lower than the temperature of the surrounding filaments, and therefore their inner densities in pressure equilibrium are expected to be only slightly higher. The clumps become denser and possibly more detectable once they enter the hotter and denser ICM, and especially as they approach the cluster core. We are encouraged by observations of H_α structures with masses of $10^6 - 10^8 M_\odot$ around the Perseus BCG (Fabian et al. 2008) but a more careful comparison needs to be made, addressing the ionization states and the radiative signature of clumps as they are disrupted and heated (Begelman & Fabian 1990; Gnat et al. 2010). One should also work out the spectrum of the X-ray emission from the multi-phased gas as it is heated by conduction and radiation.

The exact details of clump-ICM interactions, and the response of the ICM, cannot be properly addressed in 1D simulations where hydrodynamic instabilities are almost completely suppressed independent of the quenching mechanism. In this first crude study we rely on the fact that the model proposed here naturally deposits the energy over $\sim 1 \text{ kpc}$ scales (Fig. 5) in a continuous manner. Nevertheless, a realistic study of whether the gas cooling is sufficiently suppressed would require a proper 3D simulation with clump heating implemented. The inherent unstable expansion that occurs when heating is faster than the cooling is artificially damped by a 1D convection model, which introduces a free mixing-length parameter that can only be calibrated by 3D simulations. In §2.1.5 we outlined a proposed implementation of a 3D subgrid model for these clumps, which will allow all these issues to be addressed. A different kind of 2D and 3D simulations, of interactions between single clumps with the ICM gas, have been conducted in the past (Murray & Lin 2004), but not for the specific conditions of clusters, and without some of the crucial physical components such as cooling and conduction.

ACKNOWLEDGMENTS

We thank Ami Glasner for his advice on mixing-length theory. We acknowledge fruitful discussions with Peng Oh, Orly Gnat and Jerry Ostriker. This research has been partly supported by an ISF grant, by GIF grant I-895-207.7/2005, and by a DIP grant. YB is an ITC Fellow at CfA, Harvard.

REFERENCES

Balbus S. A., Reynolds C. S., 2008, *ApJ*, 681, L65
 Begelman M. C., Fabian A. C., 1990, *MNRAS*, 244, 26P
 Bertschinger E., 1985, *ApJS*, 58, 39
 Bertschinger E., Meiksin A., 1986, *ApJ*, 306, L1
 Best P. N., 2007, *New Astronomy Review*, 51, 168
 Binney J., Cowie L. L., 1981, *ApJ*, 247, 464
 Binney J., Nipoti C., Fraternali F., 2009, *MNRAS*, 397, 1804
 Birnboim Y., Dekel A., 2003, *MNRAS*, 345, 349
 Birnboim Y., Dekel A., Neistein E., 2007, *MNRAS*, 380, 339
 Birnboim Y., Keshet U., Hernquist L., 2010, *ArXiv e-prints*
 Birnboim Y., Loeb A., 2009, *Journal of Cosmology and Astro-Particle Physics*, 6, 8
 Blitz L., Spergel D. N., Teuben P. J., Hartmann D., Burton W. B., 1999, *ApJ*, 514, 818
 Bregman J. N., David L. P., 1988, *ApJ*, 326, 639
 Cattaneo A., Faber S. M., Binney J., Dekel A., Kormendy J., Mushotzky R., Babul A., Best P. N., Brüggen M., Fabian A. C., Frenk C. S., Khalatyan A., Netzer H., Mahdavi A., Silk J., Steinmetz M., Wisotzki L., 2009, *Nature*, 460, 213
 Cavagnolo K. W., Donahue M., Voit G. M., Sun M., 2009, *ApJS*, 182, 12
 Churazov E., Forman W., Vikhlinin A., Tremaine S., Gerhard O., Jones C., 2008, *MNRAS*, 388, 1062
 Ciotti L., Ostriker J. P., 2007, *ApJ*, 665, 1038
 Conroy C., Ostriker J. P., 2008, *ApJ*, 681, 151
 Conselice C. J., Gallagher III J. S., Wyse R. F. G., 2001, *AJ*, 122, 2281
 David L. P., Slyz A., Jones C., Forman W., Vrtilek S. D., Arnaud K. A., 1993, *ApJ*, 412, 479
 De Young D. S., O'Neill S. M., Jones T. W., 2008, *Extragalactic Jets: Theory and Observation from Radio to Gamma Ray*. Astronomical Society of the Pacific Conference Series, 386, 343
 Dekel A., 1981, *A&A*, 101, 79
 Dekel A., Birnboim Y., 2008, *MNRAS*, 383, 119
 Donahue M., Horner D. J., Cavagnolo K. W., Voit G. M., 2006, *ApJ*, 643, 730
 Edge A. C., Stewart G. C., Fabian A. C., Arnaud K. A., 1990, *MNRAS*, 245, 559
 El-Zant A. A., Kim W.-T., Kamionkowski M., 2004, *MNRAS*, 354, 169
 Fabian A. C., 1994, *ARA&A*, 32, 277
 Fabian A. C., 2003, *MNRAS*, 344, L27
 Fabian A. C., Johnstone R. M., Sanders J. S., Conselice C. J., Crawford C. S., Gallagher J. S. I., Zweibel E., 2008, *Nature*, 454, 968
 Faltenbacher A., Mathews W. G., 2007, *MNRAS*, 375, 313
 Field G. B., 1965, *ApJ*, 142, 531
 Fraternali F., Binney J. J., 2008, *MNRAS*, 386, 935
 Giovanelli R., Haynes M. P., Kent B. R., Saintonge A., Stierwalt S., Altaf A., Balonek T., Brosch N., Brown S., Catinella B., Furniss A., Goldstein J., Hoffman G. L., ten others 2007, *AJ*, 133, 2569
 Gnat O., Sternberg A., McKee C. F., 2010, *ArXiv e-prints*
 Guo F., Oh S. P., 2008, *MNRAS*, 384, 251
 Heckman T. M., Baum S. A., van Breugel W. J. M., McCarthy P., 1989, *ApJ*, 338, 48
 Johansson P. H., Naab T., Ostriker J. P., 2009, *ApJ*, 697, L38
 Kaufmann T., Bullock J. S., Maller A. H., Fang T., Wadsley J., 2009, *MNRAS*, 396, 191
 Kent B. R., Giovanelli R., Haynes M. P., Saintonge A., Stierwalt S., Balonek T., Brosch N., Catinella B., Koopmann R. A., Momjian E., Spekkens K., 2007, *ApJ*, 665, L15
 Kereš D., Hernquist L., 2009, *ApJ*, 700, L1
 Khochfar S., Ostriker J. P., 2008, *ApJ*, 680, 54
 Kim W.-T., El-Zant A. A., Kamionkowski M., 2005, *ApJ*, 632, 157
 Kim W.-T., Narayan R., 2003, *ApJ*, 596, 889
 Lacey C., Cole S., 1993, *MNRAS*, 262, 627
 Landau L. D., Lifshitz E. M., 1959, *Fluide Mechanics*. Pergamon press, 1959
 Leccardi A., Molendi S., 2008, *A&A*, 486, 359
 Maller A. H., Bullock J. S., 2004, *MNRAS*, 355, 694
 Markevitch M., 1998, *ApJ*, 504, 27
 Murray S. D., Lin D. N. C., 2004, *ApJ*, 615, 586
 Naab T., Johansson P. H., Ostriker J. P., Efstatouli G., 2007, *ApJ*, 658, 710
 Narayan R., Medvedev M. V., 2001, *ApJ*, 562, L129
 Neistein E., van den Bosch F. C., Dekel A., 2006, *MNRAS*, 372, 933
 Oh S. P., 2004, *MNRAS*, 353, 468
 Olano C. A., 2008, *A&A*, 485, 457
 Ostriker E. C., 1999, *ApJ*, 513, 252
 Parrish I. J., Quataert E., Sharma P., 2009, *ApJ*, 703, 96
 Parrish I. J., Stone J. M., Lemaster N., 2008, *ApJ*, 688, 905
 Popo S. B., 2000, *Turbulent Flows*. Cambridge University Press, 2000
 Press W. H., Schechter P., 1974, *ApJ*, 187, 425
 Putman M. E., Bland-Hawthorn J., Veilleux S., Gibson B. K., Freeman K. C., Maloney P. R., 2003, *ApJ*, 597, 948
 Rebusco P., Churazov E., Böhringer H., Forman W., 2006, *MNRAS*, 372, 1840
 Rosner R., Tucker W. H., 1989, *ApJ*, 338, 761
 Ruszkowski M., Oh S. P., 2010, *ApJ*, 713, 1332
 Sanderson A. J. R., Ponman T. J., O'Sullivan E., 2006, *MNRAS*, 372, 1496
 Sato K., Nagataki S., eds, 2004, *Conduction and Turbulent Mixing in Galaxy Clusters*
 Spiegel E. A., 1963, *ApJ*, 138, 216
 Spitzer L., 1962, *Physics of Fully Ionized Gases*
 Sutherland R. S., Dopita M. A., 1993, *ApJS*, 88, 253

Thom C., Peek J. E. G., Putman M. E., Heiles C.,
Peek K. M. G., Wilhelm R., 2008, ApJ, 684, 364
Voit G. M., Donahue M., 1997, ApJ, 486, 242
Wakker B. P., York D. G., Wilhelm R., Barentine J. C.,
Richter P., Beers T. C., Ivezić Ž., Howk J. C., 2008,
ApJ, 672, 298
Wang P., Abel T., 2008, ApJ, 672, 752
Zinger E., Dekel A., Kravtsov A., Birnboim Y., 2010,
in preparation